Surface & Coatings Technology 406 (2021) 126663

Contents lists available at ScienceDirect

Surface & Coatings Technology

journal homepage: www.elsevier.com/locate/surfcoat

Electrocodeposition of Ni composites and surface treatment of SiC nano-particles

S. Pinate [a,*], A. Ispas [b], P. Leisner [a], C. Zanella [a]

[a] Gjuterigatan 5, Department of Material and Manufacturing, School of Engineering, Jönköping University, Jönköping, Sweden
[b] Gustav-Kirchhoff-Str. 6, Fachgebiet Elektrochemie und Galvanotechnik, Technische Universität Ilmenau, Ilmenau, Germany

ARTICLE INFO

Keywords:
Dispersion coating
Surface treatment
ζ-Potential
Grain refinement
Microhardness

ABSTRACT

This work has explored the surface modification of SiC submicron- and nanoparticles, and its influence on the particles' chemical behaviour and deposition rate in the electroplating of composite Ni/SiC coatings. SiC particles with different sizes (50, 60, 300 and 500 nm) were codeposited in their "as-produced" state. The ζ-potential measurements and alkaline titration for the "as-produced" particles showed differences in chemical behaviour for particles of different sizes, reporting pH buffering effect, even though the particles were inert and chemically the same (SiC). A surface treatment (ST) based on nitric acid was developed in an attempt to set a similar surface state, therefore a similar chemical behaviour in all particles. The ζ-potential measurements and alkaline titration of the "surface treated" particles showed similar results, independently of the size of particles. The pH buffering effect also decreased considerably by the ST. The codeposition rate was modified by the ST differently for each size compared to their as-produced state. The content of SiC50 and SiC500 was doubled (≈2% and ≈19%), tripled for SiC300 (≈7%) and more than halved for SiC60 (≈2%). The microhardness of these composite deposits was linked to the changes in the SiC codeposition.

1. Introduction

The electrodeposition of composites rests on the successful and controlled incorporation of nanoparticles into the matrix during electroplating [1]. The purpose of this technique is to obtain nanocomposite coatings by a low-cost process with enhanced properties such as hardness, wear resistance and corrosion resistance compared to the pure metal [2,3] or composites with micro-size particles as reinforcer [4–6].

However, the production of nanocomposites is strongly dependent and sensitive to minor changes in the process' parameters [7,8], and can also produce vastly different results based on the selection of the particle [9]. Multiple studies [10–13] have pointed out how critical is the interaction of the nano-particles with the constituents of the electrolyte, and its role in the particles' incorporation. The formulation of complex electrolytes regularly includes different metallic salts, complexing agents, supporting electrolytes and additives, which in some cases can affect the behaviour of the particles in the electrolyte [14–16]. However, even in additive-free electrolytes, particles with the same nominal size also presented variations in the codeposition [17–20]. Furthermore, under the same electroplating conditions deposits with different particles' sizes resulted in significant variations in particles' content [21–23]. This suggests that differences in the particles' chemical behaviour specific to each particle size or powder batch could influence their codeposition, leading to the inconsistencies in their content when the process is replicated. Thus, decades-old of research shows often controversy on the results.

ζ-potential measurements are often used to benchmark particles' chemical behaviour and codeposition. However, it should be stressed that ζ-potential values are strongly dependent on the electrolyte's chemistry, pH and ionic strength [10,24,25], and are often measured in reference electrolytes or diluted versions of the working electrolyte [26,27]. Therefore, it is difficult to draw a comparison between studies. Thus, literature often shows contradictions between ζ-potential values even in particles with the same chemical composition [10,28–30].

The focus of this work was the study of the chemical behaviour of SiC particles different sizes (50, 60, 300 and 500 nm) and from different suppliers under the same electroplating conditions in an additive-free Ni Watt's bath. The capability of a surface treatment based on nitric acid to bring the particles independently of their size, batch, production route to a similar chemical behaviour, and its influence in the particles' codeposition rate was also studied. The particles' surface treatment presented in this work attempts for the first time to overcome the

* Corresponding author.
E-mail addresses: santiago.pinate@ju.se (S. Pinate), adriana.ispas@tu-ilmenau.de (A. Ispas), peter.leisner@ju.se (P. Leisner), caterina.zanella@ju.se (C. Zanella).

https://doi.org/10.1016/j.surfcoat.2020.126663
Received 3 September 2020; Received in revised form 17 November 2020; Accepted 18 November 2020
Available online 20 November 2020
0257-8972/© 2020 The Authors. Published by Elsevier B.V. This is an open access article under the CC BY license (http://creativecommons.org/licenses/by/4.0/).

uncertainties often given by nanopowders. Moreover, to the best of the authors' knowledge, no similar procedure has been proposed before to specifically tackle the differences in the particles' chemical interaction in the context of producing nanocomposite coatings by electroplating.

ζ-potentials measurements and alkaline titration were used to examine the behaviour of as-produced SiC particles compared to the surface-treated ones. Different composite coatings were electroplated with the different particles, both in as-produced and surfaced-treated condition. It was also studied the impact of the particles' surface treatment on the Ni matrix's microstructure and particle content, relating the effects to the coatings' microhardness.

2. Experimental and characterisation details

2.1. Electrolyte composition and experimental set-up

The electrodeposition was performed, as listed in Table I, by a direct current (DC) on low carbon sheet plates with an area of 0.15 dm^2, in a thermally controlled cell (45 °C) with 500 mL additive-free Watts bath [31]. The cell geometry was the same in all experiments. The electrode configuration was vertical and in parallel with an approximate distance between cathode and anode of 7 cm, and 1.5 cm away from a cylindric-shaped stirrer (0.7 cm diameter and 6 cm in length) placed at the bottom of the cell. Before electroplating, the substrates were mechanically ground with SiC grade #1000, cleaned ultrasonically in a diluted 5% degreaser (TICKOPUR R 33; DR H STAMM GmbH) and activated by pickling for 8 min in 2.5 M H_2SO_4. The pH of the plating electrolyte was maintained at 3.0 by adding H_2SO_4 or NaOH. The bath suspension was continuously mechanically stirred with a magnet, and additionally, ultrasounds (US) were applied for 30 min before electroplating.

Four specimens for each size were produced by adding as-produced (AP) 20 g L^{-1} of SiC particles with different average particles size: SiC50 (gnm© #SiC-110 spherical β-SiC 50 nm) presented in a previous study [32], SiC60 (Iolitec GmbH #NC-0002 spherical β-SiC 60 nm) SiC300 (ESK-SiC GmbH. NF25 spherical β-SiC 300 nm), and SiC500 (gnm© #SiC-110 irregular angular-shaped β-SiC 500 nm). Likewise, four specimens were produced with surface treated (ST) particles (Table II) from each size. The results from pure Ni coatings produced under the exact parameters (Table I) from a previous study [32] are included here as reference values.

The current efficiency (CE) was calculated as the ratio of the deposited mass minus the particles' mass (as measured by WDS) to the theoretical deposited mass as predicted by Faraday's law. The coating's thickness was approximated considering nickel's density (8.91 g cm^{-3}) and deposited mass.

2.2. Particles surface treatment

The surface treatment, based on nitric acid and described in Table II, was chosen to bring the particles to a similar oxidised surface state by removing or limiting the impact of possible surface pollutants present on the as-produced powders, e.g. partial oxidation, weakly adsorbed byproducts, or silicon compounds. Kobayashi et al. [33] used a similar surface treatment for thin film transistors, where SiO_2 layers were achieved on Si or SiC by nitric acid oxidation.

Table I
Plating bath composition and parameters.

$NiSO_4{\cdot}7H_2O$	240 g L^{-1}	Current density	DC; 4 A dm^{-2}
$NiCl_2{\cdot}6H_2O$	45 g L^{-1}	Deposition time	30 min
H_3BO_3	30 g L^{-1}	Deposits' theoretical thickness	24,5 μm
pH	3.00	Stirring speed	200 rpm
Temperature	45 °C	Cathode area	15 cm^2
Anode	Ni sheet; 99.9% purity	Particle concentration SiC particle size	20 g L^{-1} 50, 60, 300, 500 nm

Table II
Particles' surface treatment (ST).

1st step – duration: 30 min	Preparation of particle suspension in water
Filtering	
2nd step	Addition of 20 mL L^{-1} HNO_3 (65%)
3rd step – duration: 15 min	Stirring at 200 rpm
Filtering	
4th step	Rinse and filter the suspension with distilled-H_2O until the pH reaches 6.0

The AP-SiC particles were added (20 g L^{-1}) into 1 L of distilled water and stirred (200 rpm) for 30 min in order to dissolve any water-soluble residual substances from the manufacturing process. The suspension was filtered by MUNKTELL© analytical filter paper (Quality 00H, ash content 0.007%) to wash out possible dissolved compounds, maintaining at least 100 mL of suspension to avoid particle agglomeration. The suspension was set to a volume of 1 L, and 20 mL L^{-1} nitric acid (65%) was added. Afterwards, the suspension was stirred (200 rpm) for 15 min to allow a similar particles' etching. The suspension was again filtered and rinsed with distilled water until it reaches a pH of 6.0.

After the final rinsing step, the H_2O-SiC(ST) suspension was immersed immediately in the nickel bath (Table I) in order to avoid the drying and agglomeration of the particles. The thus prepared bath was ultrasound (US) for 1 h, and the pH adjusted to 3.0.

2.3. ζ-Potential and titration

The ζ-potential principle lies in measuring the potential at the upmost layer of the ionic cloud that encloses the particle, which depends on the adsorption degree of the different electrolyte's constituents [10]. To guarantee ζ-potential values close to the electrodeposition conditions, the ζ-potentials were determined with a Zetasizer Nano ZS (Malvern Instruments, Herrenberg) in a diluted (25%) Watt's electrolyte with a concentration of 0.2 g L^{-1} SiC at pH 3.0 and a temperature of 45 °C, using the principle of electrophoresis estimated by laser Doppler velocimetry.

The refraction index of the particle was set to 2.610 and the electrolyte adsorption to 0.900. The pH value was adjusted by adding H_2SO_4 or NaOH, and the particles were kept in suspension by continuous agitation and before measurements ultrasonicated for 5 min. The ζ-potential was expressed as the average value of three different sets of ten ζ-potential measurements.

The pH is expected to increase during electrodeposition due to the hydrogen reduction on the cathode surface [34]. Therefore, only an alkaline titration with NaOH 0.01 M as titrator was performed. The AP-particles (20 g L^{-1}) were added to distilled water (60 mL), the pH was measured and then adjusted to 3.0 by HCl. The titration for the ST-particles was done directly on 60 mL of the H_2O-SiC (ST) suspension.

2.4. Coating characterisation

Wavelength dispersive X-ray spectroscopy (WDS, EDAX-TSL) was preferred here for quantifying the Si particles over energy-dispersive spectroscopy (EDS), due to the higher resolution of light elements when present in low content. The weight % of Si was calculated based on Si pure standards. The analysis of the standard and each specimen was performed using an acceleration voltage of 10 kV and beam current ranging from 17.6 nA to 19.8 nA. The volume content of SiC was calculated from Si weight % and considering the particles to be stochiometric and with a density of 3.22 g cm^{-3} at 25 °C. The results are expressed as the average value of five different WDS area measurements of two different specimens.

Cross-sections in the centre of the samples were prepared as for the

electron backscattered diffraction (EBSD, EDAX-TSL) analysis, followed by mechanical polishing. The measurements were performed at a magnification of X6000 with a step size of 80 nm and with an electron probe current of approximate 4.05 nA and acceleration voltage of 15 kV. The EBSD maps were analysed in the growth direction by OIM 5™; all data points with coefficient index (CI) <0.1 were disregarded. The un-indexed phases were shown as black-coloured marks in the map, i.e. grain boundaries and codeposited particles, confirmed by energy-dispersive spectroscopy (EDS). The analysis was performed on two samples for each condition where a grain was defined as a region consisting of at least three similarly oriented connected points with a misorientation <10°. The grain size was calculated by the number of data points contained in this region and excluding twin boundaries from the calculations. The grain size was measured in the first 15 μm thickness of the deposit, measured from the substrate. The grain area average was calculated by weighting the value of the area fraction of each grain, and the grain diameter was extracted from the area by considering the grain as a circle.

The microhardness of the coatings was measured on cross sections by Vickers micro indenter (NanoTestTM Vantage) with an indentation load of 100 mN and a dwell time of 10 s. Fifteen repetitions were done on each of two specimens for each plating condition, and the hardness was express as the average and standard deviation.

3. Results and discussion

3.1. Surface treatment and chemical behaviour

The residual water after first step filtration (Table II) was translucent (Fig. 1a). The nitric acid was added, and the solution stirred. Soon after turning off the agitation, the ST-particles flocculated and sedimented (Fig. 1b) at a much faster rate, in less than a minute, compared to the AP-particles in distilled water where it took more than an hour. After the final rinsing and at pH 6.0, the flocculation and sedimentation of the ST-particles took a longer time, approximately 30 min (Fig. 1c). There was no noticeable loss of visible-sized particles in any of the rinse and filtering steps.

The ζ-potential values of the as-produced particles were negative and close to zero (Fig. 2) with a deviation of a few millivolts difference between sizes. Previous studies reported similar negative values in a different electrolytic composition. The ζ-potential of nano-SiC particles was also negative at pH 4.5 in an additive-free Watt's-Co bath [15], at pH 4 in a modified Watt's bath [16], and pH 3 in NaCl 0.01 M [35].

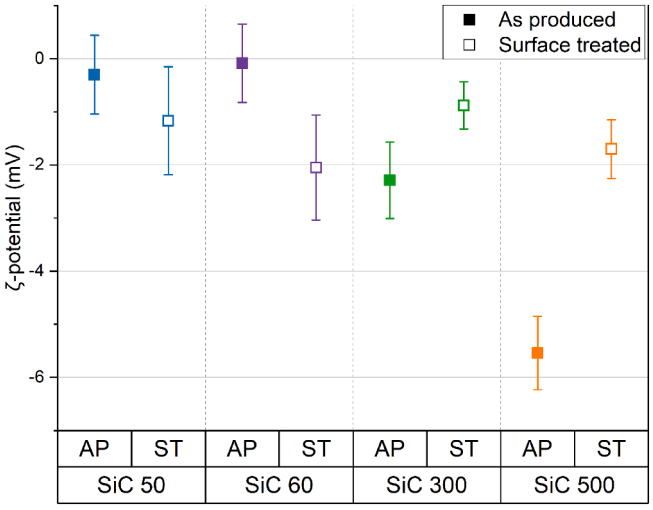

Fig. 2. ζ-potential of SiC particles (0.2 g L^{-1}) in diluted (25%) Watt's bath at pH 3, before and after surface treatment.

Nonetheless, these values were in disagreement when compared to studies reporting positive ζ-potential values [10,28,36] taken at the same pH but likewise, in different electrolytes.

The discrepancies in the AP-SiC ζ-potential values could be due to differences in their surface state, thus varying the type of surface adsorption and the particles' reaction to the medium. The 50 and 60 nm particles were more affected by the ionic strength of the Ni electrolyte leading to more unstable and closer to zero ζ-potential values. This was due to the larger specific surface area compared to the submicron particles. The ST stabilised the ζ-potential values for all the particles within the same range (Fig. 2). Therefore it seems that the ST established a comparable oxidised surface state, hence a similar chemical interaction with the electrolyte, independently of the particles size.

The titration showed significant differences in the chemical behaviour between as-produced particles (Fig. 3). This was evident immediately after being added to water, modifying the pH differently. The initial water pH was 6.0, after the addition of SiC50, the pH increased to 7.9, while after adding SiC60 up to 6.5. Hovestad et al. [24] pointed to an H^+ surface adsorption on the particles as a possible pH modifier. Differences in the surface state between nanoparticles could result in different adsorption intensity. The opposite effect was achieved with the

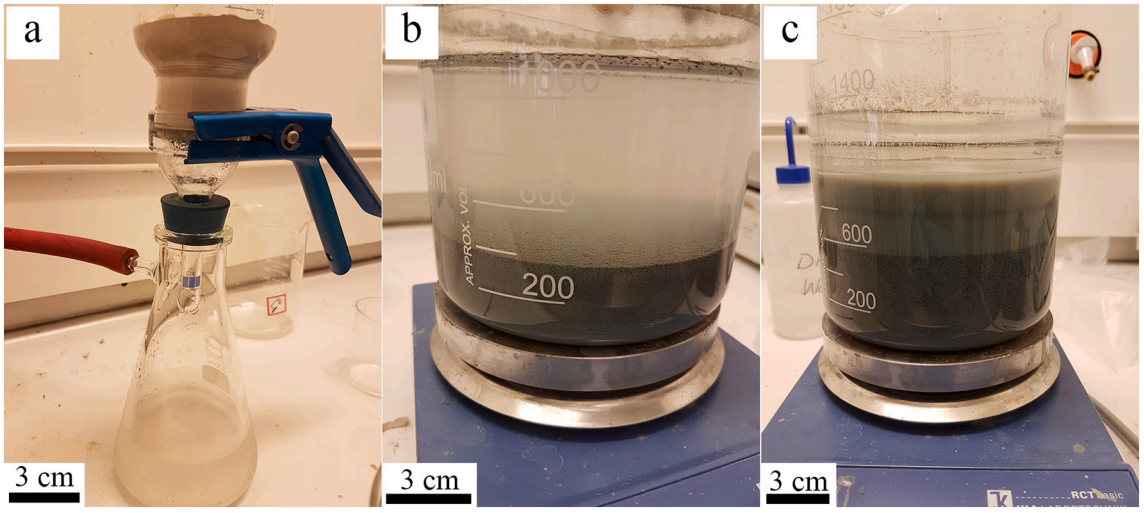

Fig. 1. The appearance of the suspension during surface treatment. (a) Immediately after the 1st filtering, (b) Immediately after HNO_3 etching and sedimentation, and (c) Immediately after the final rinse at pH 6.0.

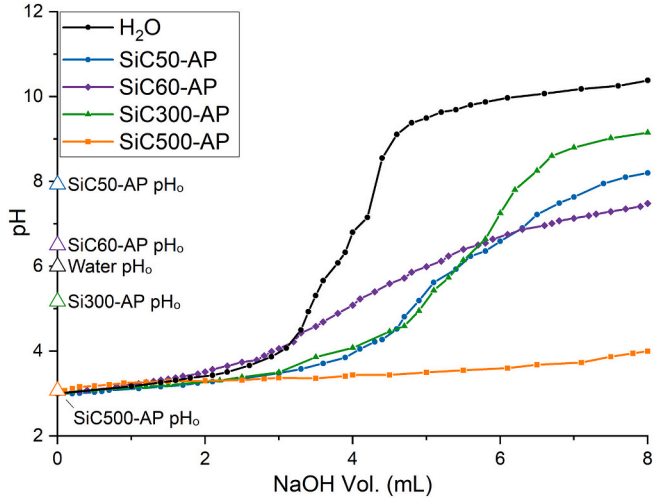

Fig. 3. Titration curves (NaOH 0.01 M) on 60 mL volume of H_2O and 20 g L^{-1} SiC: Initial pH after addition before titration and curve of AP-particles.

addition of SiC300 and SiC500, decreasing the pH, respectively, to 5.2 and 3.1 (Fig. 3). The contradiction in the values revealed differences in the particles' surface state. Due to the high specific surface area and the production methods, stabilisation and storage, particles surface may adsorb different species. The character and origin of these contaminations can also differ, i.e. weakly adsorbed ions or production byproducts, surfactants, impurities, production residues, nonstoichiometric Si (Si_xC_{1-x} or SiO_x), could modify the stability of the suspension, their codeposition and interaction with the electrolyte. This non-inert behaviour was firstly noticed by the pH changes and buffer effect (Fig. 4) in water.

A pH buffering capability was evident for all SiC particles. This could be due to desorption of H^+ from the particles' surface counteracting the addition of OH^-, slowing the pH change. Compared to water's titration curve, SiC60-AP a pH buffer effect, reporting a pH change with a less steep slope and no stabilisation plateau after the same addition of titrator volume. SiC50-AP and SiC300-AP curves showed a stronger pH buffer effect. The start of the curve slope was delayed compared to SiC60-AP. However, after pH 6 (approximately 6 mL titrator volume), the particles' buffer capacity slightly decreased compared to SiC60-AP. Both curves reached a higher pH for the same titrator volume. SiC500-AP titration curve showed the strongest pH buffering, indicating a stable pH even after the addition of 8 mL of the titrator.

The particles' surface treatment modified the type of surface adsorption-desorption, forcing a similar chemical interaction. The buffer effect for all ST-particles decreased at a similar degree (Fig. 4). The titration curves were shifted closer to water, and the slope change occurred with less addition of NaOH. Furthermore, complementary to the trend observed on ζ-potentials values, Fig. 4 shows that the surface treatment successfully brings the SiC particles independently of their size, batch, production route to a similar chemical behaviour and pH interaction.

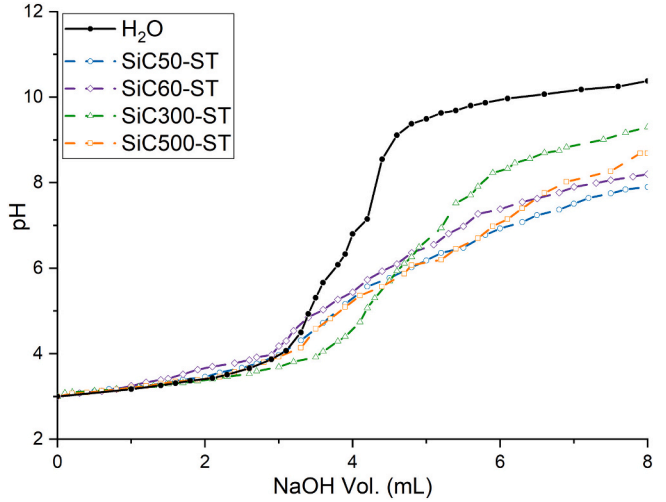

Fig. 4. Titration curves (NaOH 0.01 M) on 60 mL volume of H_2O and 20 g L^{-1} SiC-Surface treated.

3.2. Coatings electrodeposition

The variation of pH during electrodeposition was calculated by measuring it before and after the electroplating (Fig. 5). The pH increased in all cases due to hydrogen evolution [34], especially in the presence of particles compared to pure nickel. The addition of particles encouraged side reactions, i.e. hydrogen reduction, leading to the loss of the process' current efficiency (CE). The CE of pure Ni was around 98% resulting in an average thickness of ~24.1 μm. After particle addition, the CE dropped to an average of almost 95% in all cases, leading to thinner deposits with an averaged thickness of ~23.5 μm.

Pavlatou et al. [4] reported adsorption of H^+ on the surface of SiC particles in an additive-free Watts bath, which in turn, induced specific modifications in the Ni structure. The titration curves for AP-particles (Fig. 3) showed a strong effect of particles' size and the pH. A similar H^+ adsorption on the particles' surface could be possible. When the SiC particles were transported to the cathode's vicinity, the hydrogen evolution reaction would then be promoted.

The change in pH for SiC50-AP was the lowest ($\Delta pH \approx 0.09$) compared to the other particles. SiC60-AP's pH change was slightly higher ($\Delta pH \approx 0.13$) while for SiC300-AP and SiC500-AP was around 0.2. The particles' ST provoked a change in the particles' influence over the process' side reactions. The variation in pH after the electrodeposition of SiC50-ST slightly increased, while the pH variation in SiC60-ST, SiC300-ST and SiC500-ST decreased to similar values.

As previously reported by the titration curves (Fig. 4), the ST modified the surface adsorption-desorption bringing the particles to similar chemical interactions. Therefore, also affecting the extent of H^+ adsorption to similar values. Thus, promoting similar hydrogen evolution and as a result, similar pH changes.

The particles' content is reported in Table III. SiC50-AP showed a very low vol. content, close to 0.8 vol%. After ST, the codeposition rate was improved more than doubling the SiC vol. content (up to 1.7%). The EBSD map (Fig. 6b) showed that the increase in content was not due to

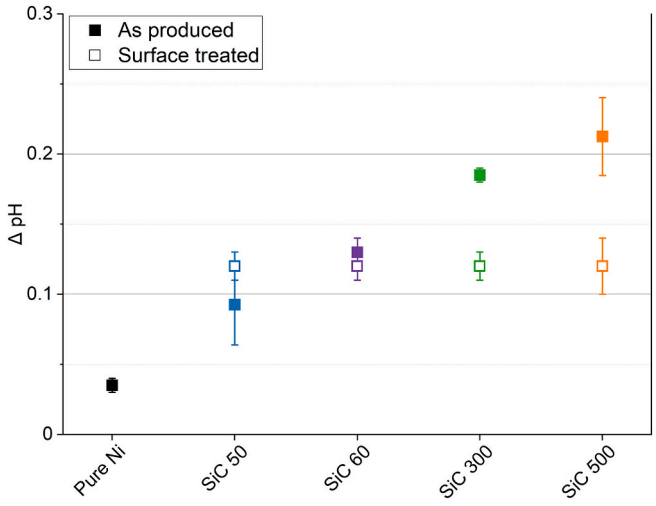

Fig. 5. pH variation after electrodeposition.

Table III
Codeposited SiC weight and volume content (%) as determined by WDS.

	SiC50		SiC60		SiC300		SiC500	
	AP	ST	AP	ST	AP	ST	AP	ST
Vol%	0.78 ± *0.13*	1.74 ± *0.35*	4.53 ± *1.54*	2.21 ± *0.31*	1.78 ± *1.06*	7.41 ± *1.65*	11.18 ± *1.15*	19.32 ± *4.00*
Wt%	0.28 ± *0.05*	0.64 ± *0.13*	1.86 ± *0.68*	0.81 ± *0.11*	0.65 ± *0.39*	2.82 ± *0.66*	4.34 ± *0.48*	8.02 ± *1.88*

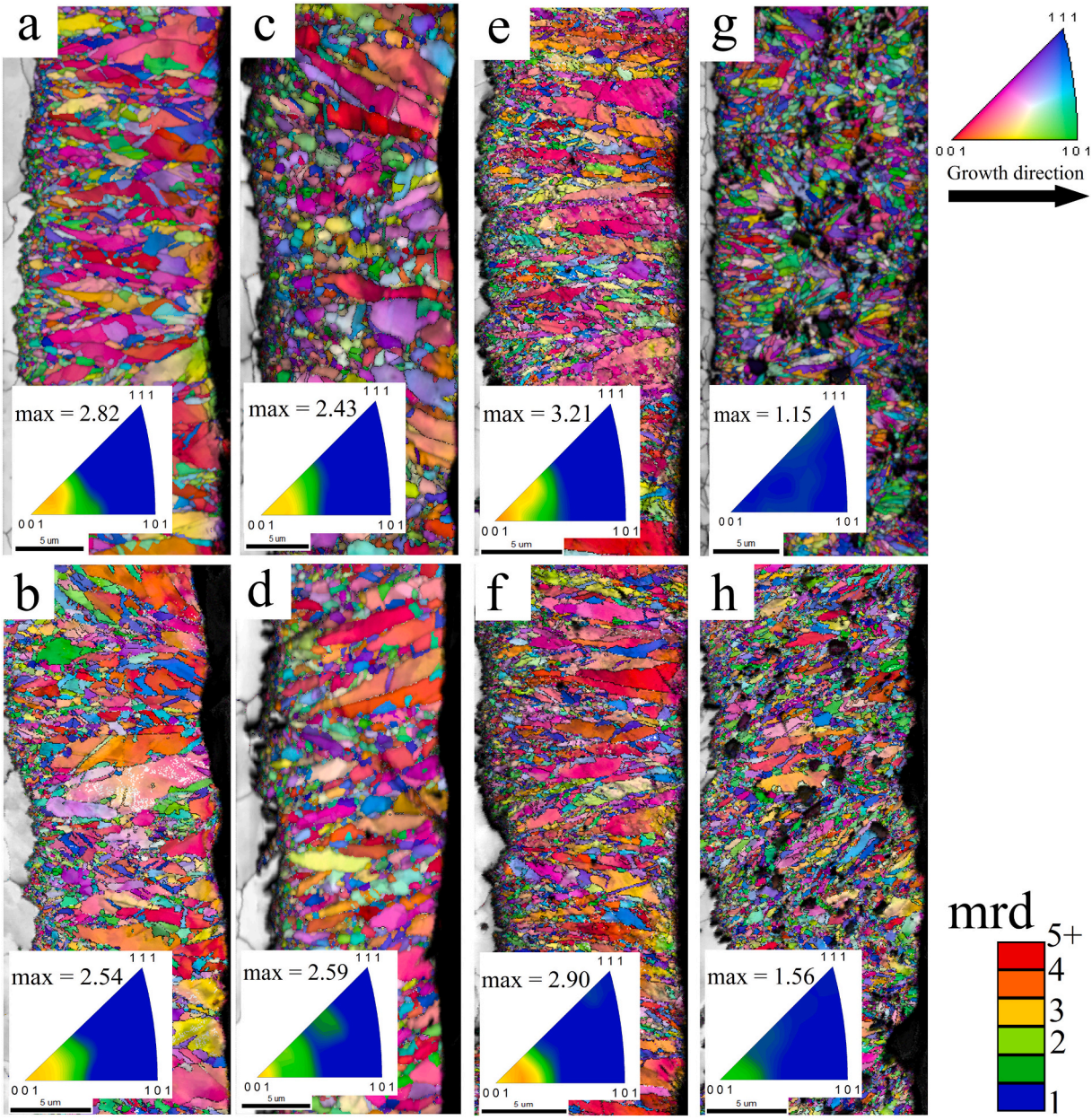

Fig. 6. Orientation map, colour-coded in relation to the electrodeposits' growth direction, shown by an arrow in the legend with the corresponding inverse pole figure, including the max texture intensity in units of multiples of random distribution (mrd) as indicated by the colour bar. (a) SiC50-AP (b) SiC50-ST (c) SiC60-AP (d) SiC60-ST (e) SiC300-AP (f) SiC300-ST (g) SiC500-AP (h) SiC500-ST.

particle agglomeration. Particles in suspension tend to form aggregates due to van der Waals attraction forces [37], leading to a major increase in their size. Therefore, if the agglomerates' size is in the submicron range, their presence would be exposed by the distinct black-coloured unindexed phase, as seen in SiC300 and SiC500 (Fig. 6). SiC60-AP codeposition rate was around 4.5 vol%. However, after ST, the content decreased, halving the value, reporting similar vol% to SiC50-ST.

SiC300-AP codeposition was less than 2 vol%. SiC300-ST reported a content increase of more than three times compared to AP. Likewise, the EBSD maps (Fig. 6f) did not show any sign of agglomeration in the electrodeposits. SiC500-AP reported the highest SiC content (11.2% vol.) compared to the rest of the AP-particles. The EBSD map (Fig. 6g) of the composite showed dispersed particles in the matrix, with some agglomerations and the incorporation of particles larger than the reported

mean diameter (500 nm). The ST appeared to decrease some of the agglomerations. However, the particle dispersion and incorporation of large particles were maintained. The codeposition was further increased to almost 20% vol.

After ST, the surface adsorption was similar, shown by similar ζ-potential values. Therefore similar negatively charged particles with similar size, ST-SiC 50 and 60 nm, reported similar codeposition. SiC60-ST decreased in volume fraction compared to AP. In the case of the submicron-particles, SiC300-ST and SiC500-ST, the ST reduced the hydrogen evolution reaction (Fig. 5). A decrease in the release of H_2 gas would allow an increase in the particles' residence time at the cathode's surface, easing their metal entrapment, thus promoting codeposition.

3.3. Microstructure

The average weighted grain size was calculated from the EBSD maps (Fig. 6). The results are reported in Table IV. The Ni deposits with AP SiC 50 and 300 nm showed a columnar growth with large elongated grains. Some grains grew uninterrupted from the substrate to surface with nano-sized grains embedded between the larger grains (Figs. 6a and e). This structure had similar characteristics to the microstructure of pure nickel reported in previous studies [2,32,38,39]. Due to the higher content of codeposited SiC60-AP, the columnar growth in these deposits was not dominant. The higher number of nano-sized particles acted as nucleation sites promoting an equiaxial-looking microstructure combined with columnar-shaped grains. The lower number of large columnar grain in SiC60-AP resulted in a more refined microstructure compared to SiC50-AP and SiC300-AP.

As previously discussed, the ST affected the codeposition rate of the particles differently. In the case of the SiC50-ST and SiC300-ST, the codeposition rate increased. Thus, the number of nucleation sites increased, promoting grain refinement. Although for SiC300-ST, this effect was minimal. SiC60-ST reported a decrease in the content of particles; therefore, compared to SiC60-AP, the grain size increased. Both SiC50-ST and SiC60-ST reported similar SiC content, and thus similar microstructure (Fig. 6b and d).

SiC500 with both AP and ST particles showed a very refined microstructure with nano-sized grains arranged in a network similar to a microstructure dominated by equiaxial growth (Fig. 6g and h). SiC500 AP and ST showed a wide particle size distribution, reporting a particles' codeposition with sizes different than the reported averaged diameter. Large particles or agglomerates, anchored on the metal surface, increase the local cathodic current density around the non-conductive particle, favouring metal nucleation rate over growth, leading to grain refinement. The deposits' inverted pole figures and the max texture intensity values are reported in Fig. 6. In all cases, except in the composites with SiC 500 nm, the ⟨100⟩ crystal orientation was preferred. This orientation is typical in the uninhibited nickel crystal growth under an electric field potential [34]. The max texture intensity of the ⟨100⟩ crystal orientation was closely related to the deposits' grain size. In deposits where the ST caused an increase in the content of the particles, ensuing grain refinement, e.g. SiC50 and SiC300, the max texture intensity decreased (Fig. 6b and f). The increase in the number of nucleation sites prompted by the particles led to the nucleation to take place on numerous atomic planes creating more randomly oriented crystals. In the composites containing SiC 60 nm, the opposite was observed. The ST decreased the particle content, leading to larger grains, therefore, a more dominant ⟨100⟩ crystal orientation.

The deposits containing SiC 500 nm showed a random crystal orientation. The growth on SiC500-AP (Fig. 6g) was preferentially random due to the combined effect of a refined structure and inhibiting species, i.e. H^+, H_{ads}, $NiOH_2$ [34]. The electrocrystallisation of nano-size grains prompted a randomly oriented microstructure. While the presence of growth inhibitors at the cathode surface also contributed to the inhibition. As observed by the pH variation (Fig. 5), the codeposition of SiC500-AP resulted in a higher increase in pH compared to other AP-particles. Thus, promoting a higher hydrogen reduction (H^+) and therefore also higher local alkalinisation leading to the formation of $NiOH_2$. Although the codeposition of ST-particles was increased, the microstructure on SiC500-ST (Fig. 6h) was somewhat less random. The codeposition of ST-particles decreased the pH variation (Fig. 5), reducing the hydrogen evolution; thus limiting the effect of the inhibiting species on the growth. Therefore, the max texture intensity partially increased.

3.4. Microhardness

Microhardness tests were performed to correlate the deposits' microhardness to the particles' content (Fig. 7) and grain refinement (Fig. 8). Tables III and IV revealed a synergistic effect between codeposition and grain size.

As previously mentioned, grain refinement was promoted by particle inclusion, due to the increase of nucleation rate over growth. The decrease in grain size, i.e. increase of grain boundaries, reinforce the metal by Hall-Petch strengthening. Moreover, the particles' codeposition promote particles-strengthening. Therefore, the increase in particles inclusion was linked to a combined increase of grain-boundary and particle-strengthening. Figs. 7 and 8 showed this relationship connected to the deposits' hardness increase, except for SiC60-AP and SiC500-AP and ST, where particle dispersion and size influenced the final hardness values.

The codeposition of SiC nano-particles on SiC50-AP was low. Therefore, the role that the particles played in the resulting microhardness was limited, and so their influence in microstructure refinement, leading to similar values as pure Ni. The ST promoted an increase in the codeposition rate, also ensuing microstructure refinement. However, in both cases, the increase was not substantial. Therefore, any strengthening was limited, leading to a low rise in hardness (ΔHV ≈ 16) for SiC50-ST compared to AP.

The combined effect of high codeposition rate linked to the resultant grain refinement led to a hardness of ≈418 HV in the SiC60-AP deposits. The resulting hardness value is more significant when compared to

Table IV
Pure Ni and composites microstructure's average grain area (GA - μm²).

	Pure Ni	SiC50	SiC60	SiC300	SiC500
As produced	9.69 ± 0.49	7.91 ± 0.45	5.93 ± 0.52	5.92 ± 0.85	1.37 ± 0.15
Surface treated	–	6.87 ± 0.33	6.37 ± 0.44	5.12 ± 0.93	0.94 ± 0.16

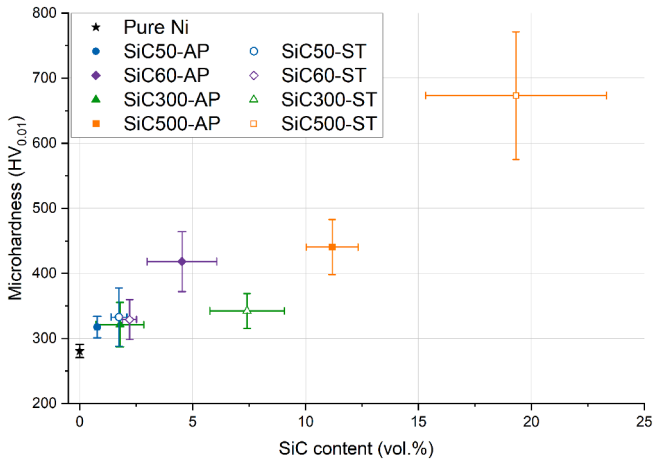

Fig. 7. Microhardness vs Codeposited SiC volume content (%) SiC before and after surface treatment as determined by WDS, as well as pure nickel.

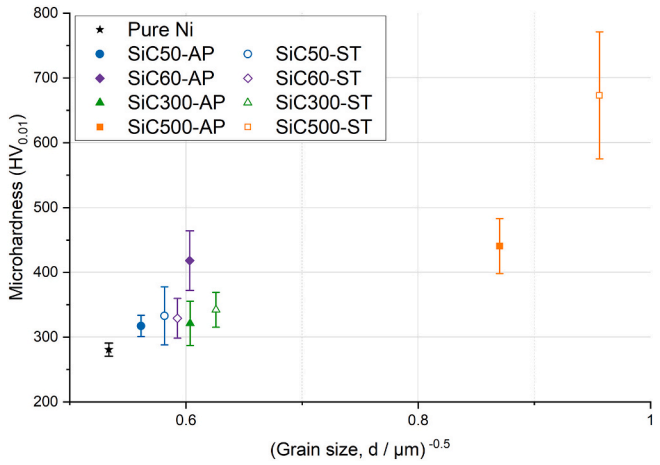

Fig. 8. Microhardness vs Grain size (diameter – μm) relationship measured for the electrodeposited composite with SiC before and after surface treatment, as well as pure nickel.

SiC300-ST with similar codeposition rate (Fig. 7) or grain size (Fig. 8). SiC60-AP hardness was higher, revealing the role of the particles' dispersion in the composite's strengthening. A higher number of entrapped nanoparticles, compared to submicron-size particles for similar volume content, could result in smaller interparticle spacing, thus providing SiC60-AP with an additional dispersion-strengthening.

SiC60's ST decreased the codeposition rate, thus the grain refinement and number of entrapped nanoparticles, reducing their strengthening contribution. SiC60-ST reported a decrease in hardness compared to AP, down to ≈329 HV, similar to values reported in SiC50-ST (≈332 HV), displaying ST's potential in providing reproducible samples independently of the powder provider, reporting similar codeposition rate, thus comparable microstructure and hardness.

The notable increase of codeposited SiC 300 nm by ST was not translated to a significant increase in deposits' microhardness compared to SiC300-AP (ΔHV ≈ 20) evidencing the already known importance of particle dispersion in the mechanical properties [40]. Particles' inclusion alone is not sufficient to further improve hardness. As previously mentioned, SiC60-AP with lower codeposition and grain refinement reported higher hardness values, due to the contribution of dispersion-strengthening. SiC500-AP reported a microhardness of around 440 HV (Fig. 7). The deposits benefited from the combined effect of high SiC content, high grain refinement, and particle dispersion; achieving the maximum hardness in the SiC-AP composites. The particles' ST promoted higher particle inclusion to almost 20% vol. content, further increasing their particle-strengthening contribution, which combined with a reduction in grain size, and particle dispersion (Fig. 6h) led to an increase in hardness to nearly 700 HV (Fig. 7), reporting the highest value among all samples.

4. Conclusions

The particles' surface was considered as one of the multiple input variables in a complex codeposition system that is often underestimated, unknown and not under control. To avoid this problem and remove the artefacts and uncertainties related to it, a surface treatment was proposed for the particles. The pretreatment of the surface of particles proved to be able to change the particles' unknown initial surface states to a consistent and reproducible one.

The ζ-potential measurements on AP-particles reported differences between sizes, showing that the type and extent of surface adsorption, in the same medium, could vary in particles with the same chemistry but different sizes. The surface treatment brought the ζ-potential to a similar value range, showing the capability of the pretreatment to bring the particles to a similar surface state, therefore similar surface adsorption.

The differences between AP-particles' was evident when suspended in water. After addition, the water's pH was modified differently for each particles' size. The titration curves proved this disparity in the chemical interaction. All AP-particles had some buffering capacity. The presence of particles, compared to water, delayed the transition to an alkaline pH. SiC500-AP showed the strongest pH buffering effect, withholding any pH change after the addition of the titrator. After the surface treatment of the particles, most of the buffering effect was removed. The titration curves for the ST-particles were similar and closer to the curve reported for water, displaying that the pretreatment successfully brought the particles independently of their size to a similar surface adsorption-desorption. Additionally, this similar behaviour was also observed during electrodeposition, where the reported pH change was alike in all ST-particles.

The pretreatment of the surface of particles proved to be beneficial in some cases to the particles codeposition rate, e.g. SiC 50, 300 and 500 nm, where the content was doubled or tripled, but detrimental to the content of codeposited SiC 60 nm, where it was halved. In the cases of SiC300-ST and SiC500-ST, the reduction in hydrogen evolution promoted particle inclusion. Most importantly, the particles' surface treatment allowed a controlled codeposition of nanoparticles with similar size, SiC 50 and 60 nm, independently of production route followed by the different suppliers. SiC50-ST and SiC60-ST reported similar ζ-potential, titration curve, pH change, codeposition rate, microstructure and microhardness.

The EBSD maps for the composites with ST-particles did not show any particle agglomeration. Therefore, the changes in content were attributed solely to the effects of the surface treatment, and not to an increase in particles total volume.

The hardness increase progression, starting from pure Ni showed a linear relationship linked to Hall-Petch and particle-strengthening mechanisms, where SiC60-AP and SiC 500 nm showed hardness values above the linear progression, evidencing further contribution by dispersion-strengthening, not observed in the rest of the samples.

The pretreatment of the surface particles proved to be an important step for removing an uncontrolled variable, making nano-SiC codeposition more reproducible. This is an essential condition for further considerations and studies on the process parameters and optimisation.

CRediT authorship contribution statement

S. Pinate: Conceptualization, Methodology, Validation, Formal analysis, Investigation, Writing - original draft, Visualization. **A. Ispas:** Validation, Investigation, Resources, Writing - review & editing. **P. Leisner:** Conceptualization, Methodology, Validation, Resources, Writing - review & editing. **C. Zanella:** Conceptualization, Methodology, Validation, Resources, Writing - review & editing, Visualization, Supervision, Project administration, Funding acquisition.

Declaration of competing interest

The authors declare that they have no known competing financial interests or personal relationships that could have appeared to influence the work reported in this paper.

Acknowledgement

The research was partially funded by the project FunDisCo (project reference number 20310117) supported by the KK-foundation, Sweden, that is kindly acknowledged. The ζ-potential measurements were performed during a short-term scientific mission fully funded by the COST Action MP1407, and hosted by the Technische Universität Ilmenau, Germany. Prof. Andreas Bund is gratefully acknowledged for making this possible.

References

[1] W. Metzger, R. Oft, G. Laux, H. Harst, Electrodeposition of dispersed layers, Galvanotek. 61 (1970) 998.

[2] C. Zanella, M. Lekka, P.L. Bonora, Influence of the particle size on the mechanical and electrochemical behaviour of micro- and nano-nickel matrix composite coatings, J. Appl. Electrochem. 39 (2009) 31–38, https://doi.org/10.1007/s10800-008-9635-y.

[3] K. Hou, M. Ger, L. Wang, S. Ke, The wear behaviour of electro-codeposited Ni–SiC composites, Wear 253 (2002) 994–1003, https://doi.org/10.1016/S0043-1648(02)00222-3.

[4] E.A. Pavlatou, M. Stroumbouli, P. Gyftou, N. Spyrellis, Hardening effect induced by incorporation of SiC particles in nickel electrodeposits, J. Appl. Electrochem. 36 (2006) 385–394, https://doi.org/10.1007/s10800-005-9082-y.

[5] M. Lekka, A. Lanzutti, C. Zanella, G. Zendron, L. Fedrizzi, P.L. Bonora, Resistance to localized corrosion of pure Ni, micro- and nano-SiC composite electrodeposits, Pure Appl. Chem. 83 (2010) 253–358, https://doi.org/10.1351/PAC-CON-10-08-21.

[6] I. Garcia, J. Fransaer, J.P. Celis, Electrodeposition and sliding wear resistance of nickel composite coatings containing micron and submicron SiC particles, Surf. Coat. Technol. 148 (2001) 171–178, https://doi.org/10.1016/S0257-8972(01)01336-6.

[7] C.T.J. Low, R.G.A. Wills, F.C. Walsh, Electrodeposition of composite coatings containing nanoparticles in a metal deposit, Surf. Coat. Technol. 201 (2006) 371–383, https://doi.org/10.1016/j.surfcoat.2005.11.123.

[8] F.C. Walsh, C. Ponce de Leon, A review of the electrodeposition of metal matrix composite coatings by inclusion of particles in a metal layer: an established and diversifying technology, Trans. IMF 92 (2014) 83–98, https://doi.org/10.1179/0020296713z.000000000161.

[9] T. Lampke, A. Leopold, D. Dietrich, G. Alisch, B. Wielage, Correlation between structure and corrosion behaviour of nickel dispersion coatings containing ceramic particles of different sizes, Surf. Coat. Technol. 201 (2006) 3510–3517, https://doi.org/10.1016/j.surfcoat.2006.08.073.

[10] M. Kenjiro, U. Takahisa, H. Tetsuya, E. Kunio, Effects of surfactants and surface treatment on aqueous dispersion of silicon carbide, Bull. Chem. Soc. Jpn. 60 (1987) 89–94, https://doi.org/10.1246/bcsj.60.89.

[11] S.H. Yeh, C.C. Wan, Codeposition of SiC powders with nickel in a Watts bath, J. Appl. Electrochem. 24 (1994) 993–1000, https://doi.org/10.1007/BF00241190.

[12] R.P. Socha, P. Nowak, K. Laajalehto, J. Väyrynen, Particle-electrode surface interaction during nickel electrodeposition from suspensions containing SiC and SiO_2 particles, Colloids Surf. A Physicochem. Eng. Asp. 235 (2004) 45–55, https://doi.org/10.1016/j.colsurfa.2004.01.011.

[13] F.C. Walsh, C.T.J. Low, J.O. Bello, Influence of surfactants on electrodeposition of a Ni-nanoparticulate SiC composite coating, Transactions of the IMF 93 (2015) 147–156, https://doi.org/10.1179/0020296715Z.000000000237.

[14] E. Rudnik, L. Burzyńska, Ł. Dolasiński, M. Misiak, Electrodeposition of nickel/SiC composites in the presence of cetyltrimethylammonium bromide, Appl. Surf. Sci. 256 (2010) 7414–7420, https://doi.org/10.1016/j.apsusc.2010.05.082.

[15] S.M. Lari Baghal, A. Amadeh, M. Heydarzadeh Sohi, S. Hadavi, The effect of SDS surfactant on tensile properties of electrodeposited Ni–Co/SiC nanocomposites, Mater. Sci. Eng. A 559 (2013) 583–590, https://doi.org/10.1016/j.msea.2012.08.145.

[16] F. Kılıç, H. Gül, S. Aslan, A. Alp, H. Akbulut, Effect of CTAB concentration in the electrolyte on the tribological properties of nanoparticle SiC reinforced Ni metal matrix composite (MMC) coatings produced by electrodeposition, Colloids Surf. A Physicochem. Eng. Asp. 419 (2013) 53–60, https://doi.org/10.1016/j.colsurfa.2012.11.048.

[17] P. Gyftou, E.A. Pavlatou, N. Spyrellis, Effect of pulse electrodeposition parameters on the properties of Ni/nano-SiC composites, Appl. Surf. Sci. 254 (2008) 5910–5916, https://doi.org/10.1016/j.apsusc.2008.03.151.

[18] T. Borkar, S.P. Harimkar, Effect of electrodeposition conditions and reinforcement content on microstructure and tribological properties of nickel composite coatings, Surf. Coat. Technol. 205 (2011) 4124–4134, https://doi.org/10.1016/j.surfcoat.2011.02.057.

[19] A. Góral, M. Nowak, K. Berent, B. Kania, Influence of current density on microstructure and properties of electrodeposited nickel-alumina composite coatings, J. Alloys Compd. 615 (2014) S406–S410, https://doi.org/10.1016/j.jallcom.2014.01.025.

[20] S. Spanou, E.A. Pavlatou, N. Spyrellis, Ni/nano-TiO_2 composite electrodeposits: textural and structural modifications, Electrochim. Acta 54 (2009) 2547–2555, https://doi.org/10.1016/j.electacta.2008.06.068.

[21] P. Gyftou, M. Stroumbouli, E.A. Pavlatou, P. Asimidis, N. Spyrellis, Tribological study of Ni matrix composite coatings containing nano and micro SiC particles, Electrochim. Acta 50 (2005) 4544–4550, https://doi.org/10.1016/j.electacta.2004.10.090.

[22] R. Starosta, A. Zielinski, Effect of chemical composition on corrosion and wear behaviour of the composite Ni–Fe–Al_2O_3 coatings, J. Mater. Process. Technol. 157-158 (2004) 434–441, https://doi.org/10.1016/j.jmatprotec.2004.09.068.

[23] T. Lampke, B. Wielage, D. Dietrich, A. Leopold, Details of crystalline growth in co-deposited electroplated nickel films with hard (nano)particles, Appl. Surf. Sci. 253 (2006) 2399–2408, https://doi.org/10.1016/j.apsusc.2006.04.060.

[24] A. Hovestad, L.J.J. Janssen, Electrochemical codeposition of inert particles in a metallic matrix, J. Appl. Electrochem. 25 (1995) 519–527, https://doi.org/10.1007/BF00573209.

[25] M. Kosmulski, J.B. Rosenholm, High ionic strength electrokinetics, Adv. Colloid Interf. Sci. 112 (2004) 93–107, https://doi.org/10.1016/j.cis.2004.09.005.

[26] D. Thiemig, R. Lange, A. Bund, Influence of pulse plating parameters on the electrocodeposition of matrix metal nanocomposites, Electrochim. Acta 52 (2007) 7362–7371, https://doi.org/10.1016/j.electacta.2007.06.009.

[27] F. Erler, C. Jakob, H. Romanus, L. Spiess, B. Wielage, T. Lampke, S. Steinhäuser, Interface behaviour in nickel composite coatings with nano-particles of oxidic ceramic, Electrochim. Acta 48 (2003) 3063–3070, https://doi.org/10.1016/S0013-4686(03)00380-3.

[28] M. Hashiba, H. Okamoto, Y. Nurishi, K. Hiramatsu, The zeta-potential measurement for concentrated aqueous suspension by improved electrophoretic mass transport apparatus – application to Al_2O_3, ZrO_3 and SiC suspensions, J. Mater. Sci. 23 (1988) 2893–2896, https://doi.org/10.1007/BF00547464.

[29] A. Bund, D. Thiemig, Influence of bath composition and pH on the electrocodeposition of alumina nanoparticles and nickel, Surf. Coat. Technol. 201 (2007) 7092–7099, https://doi.org/10.1016/j.surfcoat.2007.01.010.

[30] G. Wu, N. Li, D.L. Wang, D.R. Zhou, B.Q. Xu, K. Mitsuo, Effect of α-Al_2O_3 particles on the electrochemical codeposition of Co–Ni alloys from sulfamate electrolytes, Mater. Chem. Phys. 87 (2004) 411–419, https://doi.org/10.1016/j.matchemphys.2004.06.016.

[31] O.P. Watts, Rapid nickel plating, Trans. Am. Electrochem. Soc. 29 (1916) 395–403.

[32] S. Pinate, P. Leisner, C. Zanella, Electrocodeposition of nano-SiC particles by pulse-reverse under an adapted waveform, J. Electrochem. Soc. 166 (2019) D804–D809, https://doi.org/10.1149/2.0441915jes.

[33] H. Kobayashi, K. Imamura, W.-B. Kim, S.-S. Im, Asuha, nitric acid oxidation of Si (NAOS) method for low temperature fabrication of SiO_2/Si and SiO_2/SiC structures, Appl. Surf. Sci. 256 (2010) 5744–5756, https://doi.org/10.1016/j.apsusc.2010.03.092.

[34] J. Amblard, I. Epelboin, M. Froment, G. Maurin, Inhibition and nickel electrocrystallization, J. Appl. Electrochem. 9 (1979) 233–242, https://doi.org/10.1007/BF00616093.

[35] S.-C. Wang, W.-C.J. Wei, Electrokinetic properties of nanosized SiC particles in highly concentrated electrolyte solutions, J. Am. Ceram. Soc. 84 (2001) 1411–1414, https://doi.org/10.1111/j.1151-2916.2001.tb00852.x.

[36] S.-C. Wang, W.-C.J. Wei, Kinetics of electroplating process of nano-sized ceramic particle/Ni composite, Mater. Chem. Phys. 78 (2001) 574–580, https://doi.org/10.1016/S0254-0584(01)00564-8.

[37] H. Ohshima, Electrical Phenomena at Interfaces and Biointerfaces: Fundamentals and Applications in Nano-, Bio-, and Environmental Sciences, John Wiley & Sons, 2012.

[38] H. Alimadadi, A.B. Fanta, M.A. Somers, K. Pantleon, Crystallographic orientations and twinning of electrodeposited nickel—a study with complementary characterization methods, Surf. Coat. Technol. 254 (2016) 207–216, https://doi.org/10.1016/j.surfcoat.2014.06.013.

[39] A. Godon, J. Creus, X. Feaugas, E. Conforto, L. Pichon, C. Armand, C. Savall, Characterization of electrodeposited nickel coatings from sulphamate electrolyte without additive, Mater. Charact. 62 (2011) 164–173, https://doi.org/10.1016/j.matchar.2010.11.011.

[40] Z. Mahidashti, M. Aliofkhazraei, N. Lotfi, Review of nickel-based electrodeposited tribo-coatings, Trans. Indian Inst. Metals 71 (2018) 257–295, https://doi.org/10.1007/s12666-017-1175-x.